Stress intensity factor for multiple inclined or curved cracks problem in circular positions in plane elasticity

R. A. Rafar[1], **N. M. A. Nik Long**[1,2,*], **N. Senu**[1,2], **and N. A. Noda**[3]

[1] Mathematics Department, Faculty of Science, Universiti Putra Malaysia, 43400 Serdang, Selangor, Malaysia
[2] Institute for Mathematical Research, Universiti Putra Malaysia, Serdang, Selangor, Malaysia
[3] Kyushu Institute of Technology, Kitakyushu, Japan

Received 19 December 2016, revised 14 April 2017, accepted 5 May 2017
Published online 9 June 2017

Key words Stress intensity factor, multiple inclined or curved cracks, circular position, hypersingular integral equation.

The problems of multiple inclined or curved cracks in circular positions is treated by using the hypersingular integral equation method. The cracks center are placed at the edge of a virtual circle with radius R. The first crack is fixed on the x-axis while the second crack is located on the boundary of a circle with the varying angle, θ. A system of hypersingular integral equations is formulated and solved numerically for the stress intensity factor (SIF). Numerical examples demonstrate the effect of interaction between two cracks in circular positions are given. It is found that, the severity at the second crack tips are significant when the ratio length of the second to the first crack is small and it is placed at a small angle of θ.

1 Introduction

The multiple cracks problems that involved arbitrarily crack arrangement are common in many engineering structures. Therefore there is a need to study the interaction between two arbitrary cracks configuration in order to explain the stress distribution in the vicinity of two cracks and their effect on strength. The multiple two dimensional problems of inclined and curved cracks can be investigated by determining the stress intensity factor (SIF). In previous years, Vialaton et al. [8] used the complex potential method to determine the SIF for two identical length of collinear cracks in an infinite plate under arbitrary concentrated loading. With the help of superposition technique, Kachanov [10, 11] showed that the solution of interaction of multiple cracks problems leads in solving the system of linear algebraic equations. Furthermore, many researchers used the integral equation methods for the numerical solution of multiple cracks problems. For example, Panasyuk et al. [9] presented a singular integral equation using a perturbation method to solve multiple cracks problems. Chen [12] used the complex variable function method to formulate the singular integral equation for multiple curved cracks problems. In addition, Chen and Lin [13] investigated the multiple curved branch-cracks in term of singular integral equation. Helsing [14] proposed a scheme for the numerical solution of singular integral equations on piecewise smooth curves. Chen [17] and Chen et al. [2] used the Fredholm integral equation to solve multiple cracks problems. Hypersingular integral equation has also been used to solve the multiple cracks problems. For example, Chen [18] solved the hypersingular integral equation in a closed form which the unknowns are approximated by a weight function multiplied by a polynomial. In addition, Nik Long and Eshkuvatov [3], Aridi et al. [20] and Nik Long et al. [5] used the complex variable function method to formulate the hypersingular integral equation. The curved length coordinate method is then used to solve the hypersingular integral equation numerically. Zozulya [21] developed hypersingular integral regularization and applied it for the case of three dimensional crack problem. Moreover, Wang et al. [22] used hypersingular integral equation to formulate and solve the micromechanical models. In addition, there are more cracks problems that were solved using the hypersingular integral equations [23–30].

Formulation in terms of hypersingular integral equation for solving the problem of multiple inclined or curved cracks in circular positions in plane elasticity is studied in this paper. Numerical examples are given to show the behavior of the SIF at the crack tips, and are presented and displayed graphically.

* Corresponding author, E-mail: nmasri@upm.edu.my, Phone: +603-8946 6811, Fax: +603-8943 7958

2 Problem statement and formulation

The stresses $(\sigma_x, \sigma_y, \sigma_{xy})$, the resultant force functions (X, Y) and the displacements (u, v) are related to the complex potentials $\Phi(z)$ and $\Psi(z)$ as follows [1]

$$\sigma_x + \sigma_y = 4\mathrm{Re}\Phi(z), \tag{1}$$

$$\sigma_y - \sigma_x + 2i\sigma_{xy} = 2[\bar{z}\Phi'(z) + \Psi(z)], \tag{2}$$

$$f = -Y + iX = \phi(z) + z\overline{\phi'(z)} + \overline{\psi(z)} + c, \tag{3}$$

$$2G(u + iv) = K\phi(z) - z\overline{\phi'(z)} + \psi(z), \tag{4}$$

where $\Phi(z) = \phi'(z)$ and $\Psi(z) = \psi'(z)$, G is shear modulus of elasticity, $K = (3 - v)/(1 + v)$ for plane stress, $K = 3 - v$ for plane strain, v as Poisson's ratio, and $z = x + iy$. The derivative in a specified direction (abbreviated as DISD) is defined as

$$\begin{aligned}\frac{d}{dz}\{-Y + iX\} &= \Phi(z) + \overline{\Phi(z)} + \frac{d\bar{z}}{dz}\left(z\overline{\Phi'(z)} + \overline{\Psi(z)}\right)\\ &= N + iT,\end{aligned} \tag{5}$$

where $N + iT$ denotes the normal and tangential tractions along the segment $\overline{z, z + dz}$ which can be determined from Fig. 1. The value of $N + iT$ depends on both the position of point z as well as on the direction of the segment $d\bar{z}/dz$ [2,3].

It is known that the formulation for single inclined and single curved crack problem in term of hypersingular integral equation is [19]

$$\frac{1}{\pi}\oint\!\!\!\!\!\!-_L \frac{g(t)dt}{(t - t_0)^2} + \frac{1}{2\pi}\int_L K_1(t, t_0)g(t)dt + \frac{1}{2\pi}\int_L K_2(t, t_0)\overline{g(t)}dt = N(t_0) + iT(t_0), \quad t_0 \in L, \tag{6}$$

where

$$\begin{aligned}K_1(t, t_0) &= -\frac{1}{(t - t_0)^2} + \frac{1}{(\bar{t} - \bar{t}_0)^2}\frac{d\bar{t}_0}{dt_0}\frac{d\bar{t}}{dt},\\ K_2(t, t_0) &= -\frac{1}{(\bar{t} - \bar{t}_0)^2}\left(\frac{d\bar{t}}{dt} + \frac{d\bar{t}_0}{dt_0}\right) - \frac{2(t - t_0)}{(\bar{t} - \bar{t}_0)^3}\frac{d\bar{t}_0}{dt_0}\frac{d\bar{t}}{dt},\end{aligned}$$

and $g(t)$ is the crack opening displacement (COD) distribution along the crack. It is also known that $g(t)$ has the following properties:

$$\begin{aligned}&g(t) = O[\sqrt{t - t_{A_j}}] \text{ at the crack tip } A_j, \quad j = 1, 2,\\ &g(t) = O[\sqrt{t - t_{B_j}}] \text{ at the crack tip } B_j, \quad j = 1, 2.\end{aligned} \tag{7}$$

In Eq. (6), the first term is hypersingular integral and it is defined as a Hadamart finite part integral.

Consider two inclined cracks (Fig. 1) lie on the boundary of a virtual circular with radius R subjected to $\sigma_x^\infty = \sigma_y^\infty = p$. By applying the superposition principle on $g_1(t_1)$ along L_1 and $g_2(t_2)$ along L_2, the hypersingular integral equation is obtained as

$$\begin{aligned}&\frac{1}{\pi}\oint\!\!\!\!\!\!-_{L_1} \frac{g_1(t_1)dt_1}{(t_1 - t_{10})^2} + \frac{1}{2\pi}\int_{L_1} K_1(t_1, t_{10})g_1(t_1)dt_1 + \frac{1}{2\pi}\int_{L_1} K_2(t_1, t_{10})\overline{g_1(t_1)}dt_1 + \frac{1}{\pi}\int_{L_2}\frac{g_2(t_2)dt_2}{(t_2 - t_{10})^2}\\ &\quad + \frac{1}{2\pi}\int_{L_2} K_1(t_2, t_{10})g_2(t_2)dt_2 + \frac{1}{2\pi}\int_{L_2} K_2(t_2, t_{10})\overline{g_2(t_2)}dt_2 = N_1(t_{10}) + iT_1(t_{10}),\end{aligned} \tag{8}$$

where $N_1(t_{10}) + iT_1(t_{10})$ is the traction applied at point t_{10} caused by COD function, $g_1(t_1)$, on L_1, and

$$\begin{aligned}K_1(t_1, t_{10}) &= -\frac{1}{(t_1 - t_{10})^2} + \frac{1}{(\bar{t}_1 - \bar{t}_{10})^2}\frac{d\bar{t}_{10}}{dt_{10}}\frac{d\bar{t}_1}{dt_1},\\ K_2(t_1, t_{10}) &= -\frac{1}{(\bar{t}_1 - \bar{t}_{10})^2}\left(\frac{d\bar{t}_1}{dt} + \frac{d\bar{t}_{10}}{dt_{10}}\right) - \frac{2(t_1 - t_{10})}{(\bar{t}_1 - \bar{t}_{10})^3}\frac{d\bar{t}_{10}}{dt_{10}}\frac{d\bar{t}_1}{dt_1},\end{aligned}$$

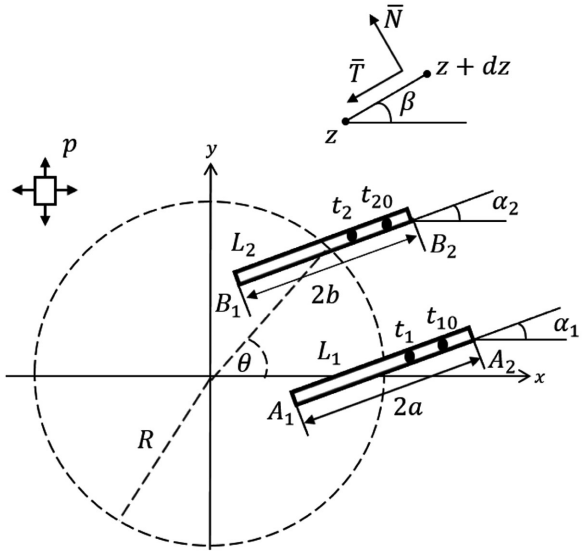

Fig. 1 Two inclined cracks placed in a circular position in plane elasticity.

$$K_1(t_2, t_{10}) = -\frac{1}{(t_2 - t_{10})^2} + \frac{1}{(\bar{t}_2 - \bar{t}_{10})^2}\frac{d\bar{t}_{10}}{dt_{10}}\frac{d\bar{t}_2}{dt_2},$$

$$K_2(t_2, t_{10}) = -\frac{1}{(\bar{t}_2 - \bar{t}_{10})^2}\left(\frac{d\bar{t}_2}{dt_2} + \frac{d\bar{t}_{10}}{dt_{10}}\right) - \frac{2(t_2 - t_{10})}{(\bar{t}_2 - \bar{t}_{10})^3}\frac{d\bar{t}_{10}}{dt_{10}}\frac{d\bar{t}_2}{dt_2}.$$

Similarly, the hypersingular integral equation for L_2 is

$$\frac{1}{\pi}\oint_{L_2}\frac{g_2(t_2)dt_2}{(t_2 - t_{20})^2} + \frac{1}{2\pi}\int_{L_2} K_1(t_2, t_{20})g_2(t_2)dt_2 + \frac{1}{2\pi}\int_{L_2} K_2(t_2, t_{20})\overline{g_2(t_2)}dt_2 + \frac{1}{\pi}\int_{L_1}\frac{g_1(t_1)dt_1}{(t_1 - t_{20})^2}$$
$$+ \frac{1}{2\pi}\int_{L_1} K_1(t_1, t_{20})g_1(t_1)dt_1 + \frac{1}{2\pi}\int_{L_1} K_2(t_1, t_{20})\overline{g_1(t_1)}dt_1 = N_2(t_{20}) + iT_2(t_{20}), \tag{9}$$

where $N_2(t_{20}) + iT_2(t_{20})$ is the traction applied at point t_{20} caused by COD function, $g_1(t_1)$, on L_2 and

$$K_1(t_2, t_{20}) = -\frac{1}{(t_2 - t_{20})^2} + \frac{1}{(\bar{t}_2 - \bar{t}_{20})^2}\frac{d\bar{t}_{20}}{dt_{20}}\frac{d\bar{t}_2}{dt_2},$$

$$K_2(t_2, t_{20}) = -\frac{1}{(\bar{t}_2 - \bar{t}_{20})^2}\left(\frac{d\bar{t}_2}{dt_2} + \frac{d\bar{t}_{20}}{dt_{20}}\right) - \frac{2(t_2 - t_{20})}{(\bar{t}_2 - \bar{t}_{20})^3}\frac{d\bar{t}_{20}}{dt_{20}}\frac{d\bar{t}_2}{dt_2},$$

$$K_1(t_1, t_{20}) = -\frac{1}{(t_1 - t_{20})^2} + \frac{1}{(\bar{t}_1 - \bar{t}_{20})^2}\frac{d\bar{t}_{20}}{dt_{20}}\frac{d\bar{t}_1}{dt_1},$$

$$K_2(t_1, t_{20}) = -\frac{1}{(\bar{t}_1 - \bar{t}_{20})^2}\left(\frac{d\bar{t}_1}{dt_1} + \frac{d\bar{t}_{20}}{dt_{20}}\right) - \frac{2(t_1 - t_{20})}{(\bar{t}_1 - \bar{t}_{20})^3}\frac{d\bar{t}_{20}}{dt_{20}}\frac{d\bar{t}_1}{dt_1}.$$

Equations (8) and (9) are solved for $g_1(t_1)$ and $g_2(t_2)$ concurrently.

3 Numerical examples

In solving Eqs. (8) and (9), we used the curved length coordinate method which transform the integral along the curves into the real axis with interval of $2a$ and $2b$ by using the mapping functions $t_1(s_1)$ and $t_2(s_2)$, respectively. The functions $g_1(t_1)$ and $g_2(t_2)$ can be defined as follows [12, 19]

$$g_1(t_1)|_{t_1 = t_1(s_1)} = \sqrt{a^2 - s_1^2}H_1(s_1), \tag{10}$$

$$g_2(t_2)|_{t_2 = t_2(s_2)} = \sqrt{b^2 - s_2^2}H_2(s_2), \tag{11}$$

where $H_1(s_1) = H_{11}(s_1) + iH_{12}(s_1)$ and $H_2(s_2) = H_{21}(s_2) + iH_{22}(s_2)$. Using these conversions, the system of integral equations in (8) and (9) can be evaluate numerically as in [3, 12, 19]. The quadrature rules by Mayrhofer and Fisher [4] which are used for solving the integral equations is described in the Appendix.

The stress intensity factor (SIF) at the crack tips can be evaluated respectively [3]

$$(K_1 - iK_2)_{A_j} = \sqrt{2\pi} \lim_{t_1 \to t_{A_j}} \sqrt{|t_1 - t_{A_j}|} g_1'(t_1), \quad j = 1, 2, \tag{12}$$

and

$$(K_1 - iK_2)_{B_j} = \sqrt{2\pi} \lim_{t_2 \to t_{B_j}} \sqrt{|t_2 - t_{B_j}|} g_2'(t_2), \quad j = 1, 2, \tag{13}$$

where $g_1'(t_1)$ and $g_2'(t_2)$ are obtained by solving Eqs. (8) and (9) simultaneously.

3.1 Example 1

Consider the interaction between two inclined cracks in circular positions in an infinite plate. For comparison purposes, two inclined cracks are under uniaxial tension $\sigma_y^\infty = p$ (Fig. 2). Both cracks are placed on the boundary of the virtual circle where the second crack, L_2, lies at an angle $\theta = 180^\circ$. The SIFs at the crack tips A_1, A_2, B_1, and B_2 are expressed as

$$\begin{aligned} K_{iA_j} &= F_{iA_j}(2a/d)p\sqrt{\pi a}, \\ K_{iB_j} &= F_{iB_j}(2a/d)p\sqrt{\pi b} \quad i, j = 1, 2. \end{aligned} \tag{14}$$

Table 1 shows the calculated values of F_{1B_1} and F_{1B_2}, and $a = b$. It exhibits that our results have a good agreement with those of [7].

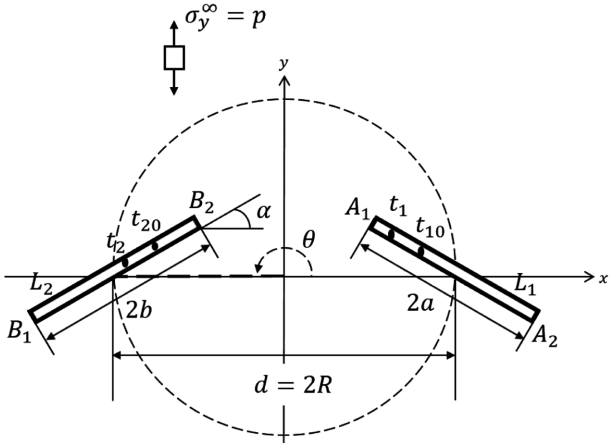

Fig. 2 Two inclined cracks with equal length lie on the virtual circular boundary with radius R.

Figs. 3 and 4 plot the nondimensional SIF against the angle of positions of second crack, θ, for two inclined cracks with the angle of inclination is $\alpha_1 = \alpha_2 = 20^\circ$ and 60°, respectively, (Fig. 1). The calculated SIFs at the crack tips A_1, A_2, B_1, and B_2 are defined as

$$\begin{aligned} K_{iA_j} &= F_{iA_j}(\theta, b/a)p\sqrt{\pi a}, \\ K_{iB_j} &= F_{iB_j}(\theta, b/a)p\sqrt{\pi b}, \quad i, j = 1, 2. \end{aligned} \tag{15}$$

In Fig. 3, for the case $b/a = 0.1$, since the second crack is much smaller than the first crack, the nondimensional SIFs at the first crack tips (Figs. 3 a and 3 b) are not fluctuating significantly, while the nondimensional SIFs at the second crack tips (Figs. 3 c and 3 d) are varying significantly. The shielding effect on the second crack tips (Figs. 3 c and 3 d) for $b/a = 0.5$ and 1.0 is found to be more stronger than the first crack tips (Figs. 3 a and 3 b) with an increasing angle θ. The finding shows that the severity on the second crack is obvious as its length is half or equal to the first crack length.

Table 1 A comparison of the nondimensional SIFs for two inclined cracks in an infinite plate with the previous numerical computation (Fig. 2).

	$\alpha = 20^\circ$				$\alpha = 30^\circ$			
$2a/d$	$F_{1B_1}{}^{*}$	$F_{1B_1}{}^{**}$	$F_{1B_2}{}^{*}$	$F_{1B_2}{}^{**}$	$F_{1B_1}{}^{*}$	$F_{1B_1}{}^{**}$	$F_{1B_2}{}^{*}$	$F_{1B_2}{}^{**}$
0.1	0.8839	0.8847	0.8839	0.8847	0.7513	0.7503	0.7502	0.7503
0.2	0.8861	0.8866	0.8870	0.8877	0.7514	0.7516	0.7520	0.7522
0.3	0.8898	0.8900	0.8927	0.8934	0.7537	0.7534	0.7560	0.7559
0.4	0.8950	0.8956	0.9021	0.9027	0.7559	0.7560	0.7620	0.7620
0.5	0.9016	0.9023	0.9169	0.9175	0.7596	0.7595	0.7718	0.7718
0.6	0.9102	0.9108	0.9398	0.9404	0.7642	0.7640	0.7872	0.7871
0.7	0.9213	0.9218	0.9763	0.9767	0.7701	0.7698	0.8110	0.8110
0.8	0.9359	0.9363	1.0381	1.0382	0.7777	0.7775	0.8492	0.8490
0.9	0.9570	0.9570	1.1590	1.1600	0.7886	0.7881	0.9140	0.9140
1.0	0.9947		1.5124		0.8060		1.0465	
1.1					0.8382		1.4528	

* Present method
** Denda and Dong [7]

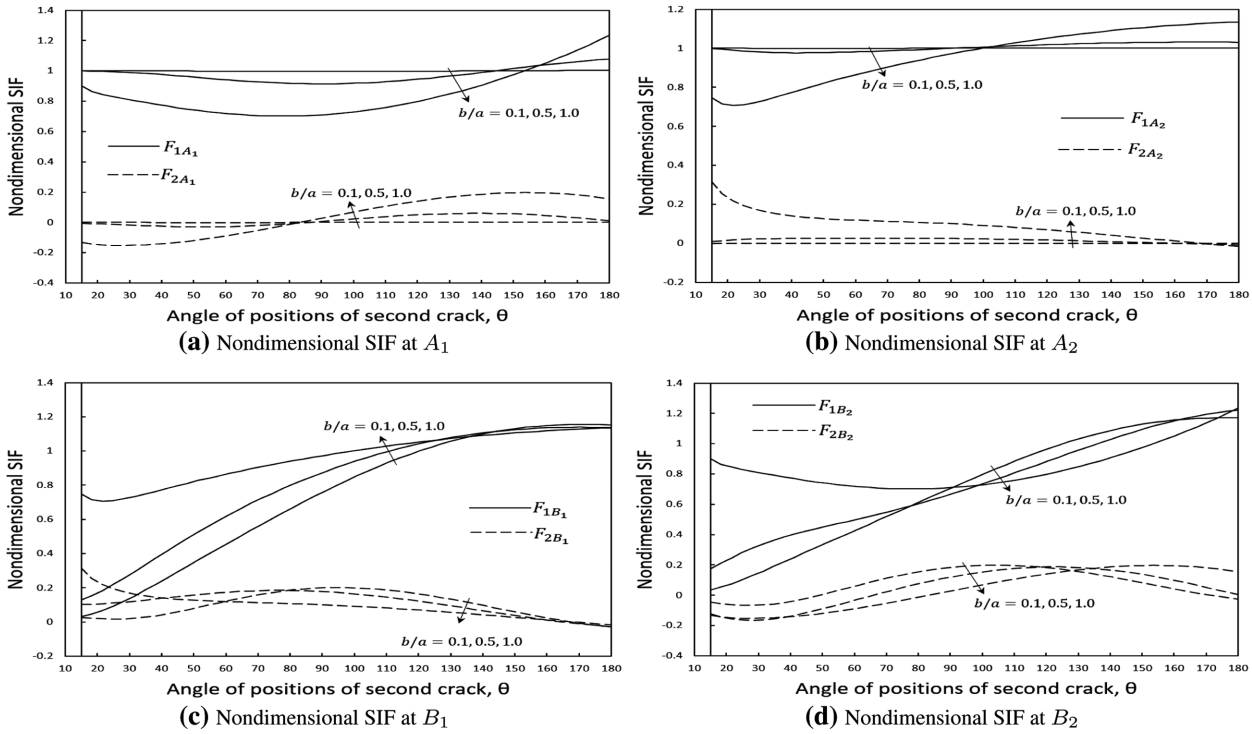

(a) Nondimensional SIF at A_1 **(b)** Nondimensional SIF at A_2

(c) Nondimensional SIF at B_1 **(d)** Nondimensional SIF at B_2

Fig. 3 Nondimensional SIF for two inclined cracks with $\alpha_1 = \alpha_2 = 20^\circ$ when θ is changing (Fig. 1).

Fig. 4 shows that the shielding effect on the second crack tips (Figs. 4 c and 4 d) is more significant than the first crack tips (Figs. 4 a and 4 b). These observations show that the second crack is most affected as the angle θ increased. In addition, the severity on the second crack for $\alpha_1 = \alpha_2 = 60^\circ$ (Fig. 4) is more serious than $\alpha_1 = \alpha_2 = 20^\circ$ (Fig. 3). For example, in the case of $b/a = 0.1$ and $\theta = 48^\circ$, the results for $\alpha_1 = \alpha_2 = 60^\circ$ are $F_{1B_1} = 0.38690$ and $F_{1B_2} = 0.49104$, while for $\alpha_1 = \alpha_2 = 20^\circ$, we have $F_{1B_1} = 0.32533$ and $F_{1B_2} = 0.31436$.

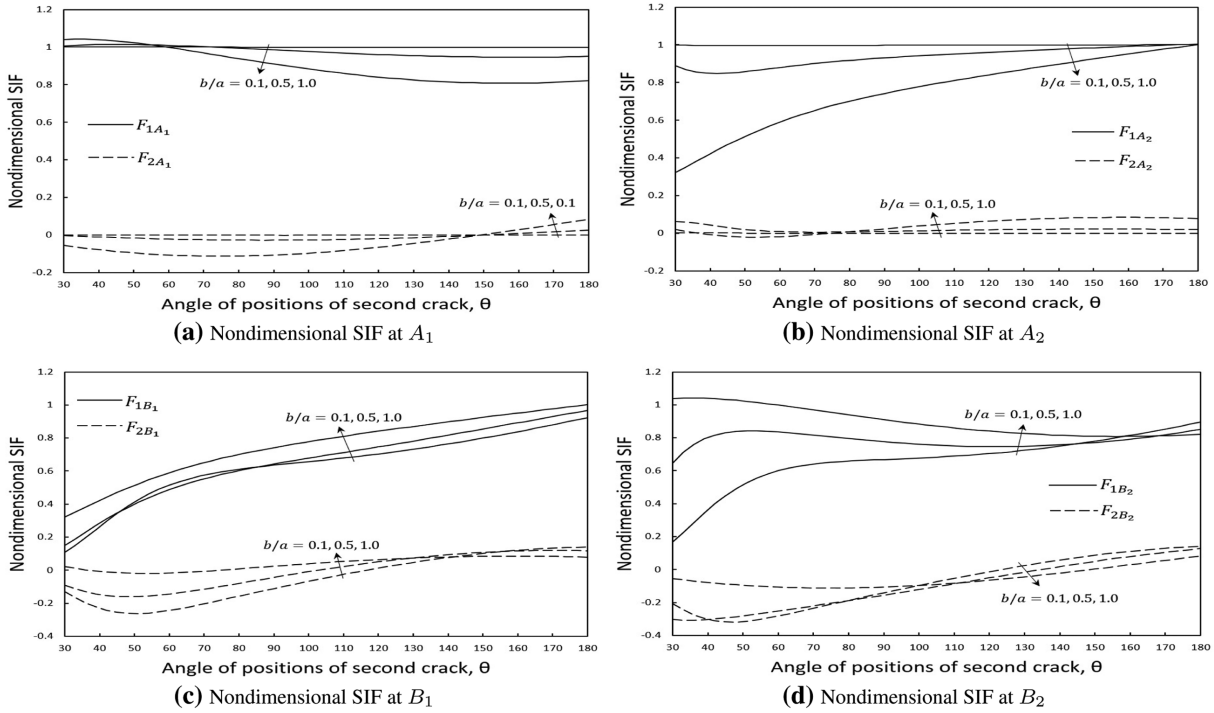

(a) Nondimensional SIF at A_1 **(b)** Nondimensional SIF at A_2

(c) Nondimensional SIF at B_1 **(d)** Nondimensional SIF at B_2

Fig. 4 Nondimensional SIF for two inclined cracks with $\alpha_1 = \alpha_2 = 60^\circ$ and θ varies (Fig. 1).

Fig. 5 represents the nondimensional SIF versus the ratio b/a for $\alpha_1 = \alpha_2 = 20^\circ$. It can be seen that the crack tips has the higher value of F_1 at the angle $\theta = 180^\circ$ than at the angle $\theta = 15^\circ$ and 90°. That is to say, both cracks have more shielding effect at the angle $\theta = 180^\circ$. In addition, at an angle $\theta = 15^\circ$, the values of F_{1A_1} and F_{1A_2} decreased whereas the values of F_{1B_1} and F_{1B_2} increased as the ratio b/a increased. These observations show that at an angle $\theta = 15^\circ$, as the length of the second crack increases, the severity at the second crack tips is more significant than the first.

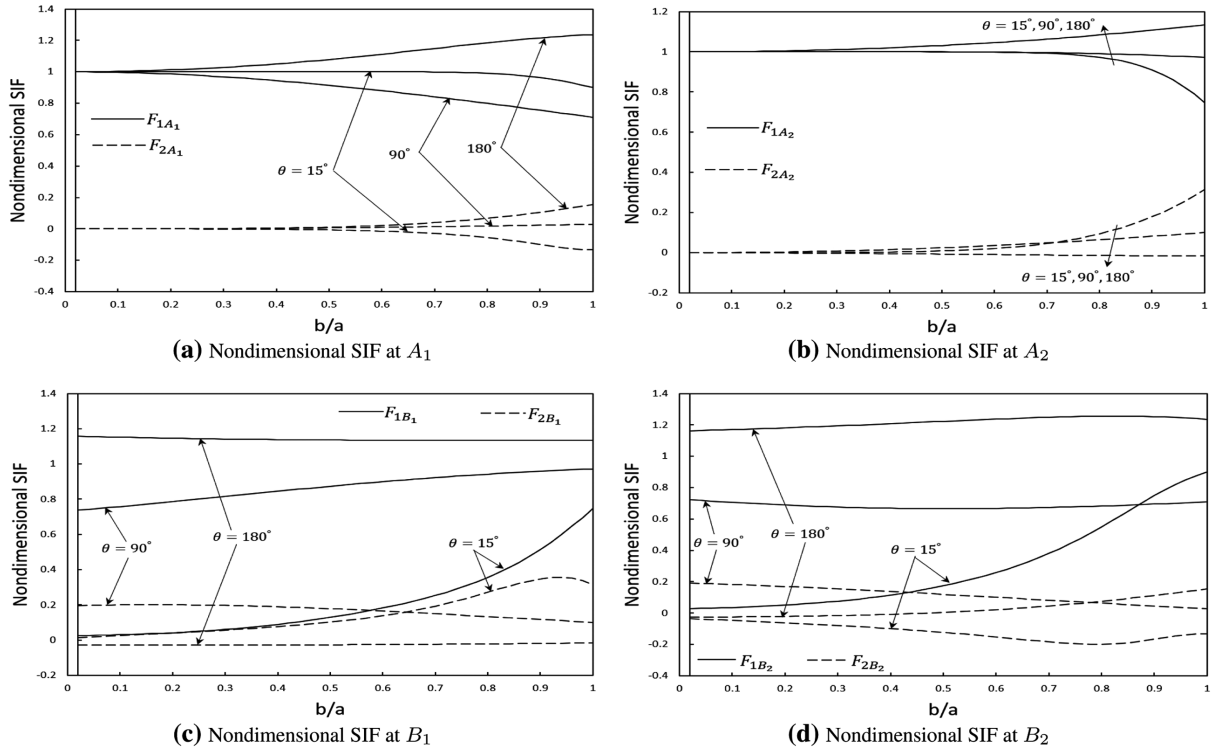

(a) Nondimensional SIF at A_1 **(b)** Nondimensional SIF at A_2

(c) Nondimensional SIF at B_1 **(d)** Nondimensional SIF at B_2

Fig. 5 Nondimensional SIF for two inclined cracks when $\alpha_1 = \alpha_2 = 20^\circ$ as b/a changing (Fig. 1).

3.2 Example 2

Consider two curved cracks subjected to the remote tension $\sigma_x^\infty = \sigma_y^\infty = p$ (Figs. 6 and 7). The radius of L_1 and L_2 is denoted as R_1 and R_2 with length $2a$ and $2b$, respectively. The calculated results for the SIFs at crack tips A_1, A_2, B_1, and B_2 are

$$\begin{aligned} K_{iA_j} &= F_{iA_j}(\theta, R_2/R_1)p\sqrt{\pi a}, \\ K_{iB_j} &= F_{iB_j}(\theta, R_2/R_1)p\sqrt{\pi b}, \quad i, j = 1, 2. \end{aligned} \tag{16}$$

The obtained results for the problems in Fig. 6 for $R_1/R = 0.9$ and $\theta = 180^\circ$ are listed in Table 2.

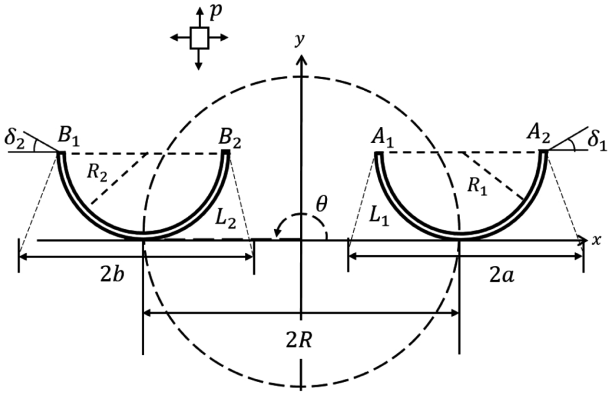

Fig. 6 Two curved cracks in an infinite plate.

Table 2 Nondimensional SIFs for the problem shown in Fig. 6.

R_2/R_1	F_{1A_1}	F_{2A_1}	F_{1A_2}	F_{2A_2}	F_{1B_1}	F_{2B_1}	F_{1B_2}	F_{2B_2}
0.1	0.3753	-0.3776	0.3764	0.3775	0.3030	-0.4386	0.3286	0.4598
0.2	0.3725	-0.3797	0.3764	0.3788	0.3165	-0.4415	0.3166	0.4663
0.3	0.3685	-0.3840	0.3763	0.3809	0.3294	-0.4425	0.3039	0.4729
0.4	0.3643	-0.3912	0.3763	0.3840	0.3416	-0.4421	0.2908	0.4798
0.5	0.3605	-0.4017	0.3764	0.3882	0.3529	-0.4410	0.2772	0.4863
0.6	0.3582	-0.4163	0.3770	0.3936	0.3632	-0.4388	0.2642	0.4923
0.7	0.3580	-0.4358	0.3785	0.4003	0.3726	-0.4365	0.2539	0.4978
0.8	0.3607	-0.4614	0.3814	0.4086	0.3812	-0.4345	0.2511	0.5027
0.9	0.3631	-0.4937	0.3866	0.4189	0.3888	-0.4327	0.2678	0.5084
1.0	0.3297	-0.5316	0.3949	0.4324	0.3949	-0.4324	0.3297	0.5316

For the problem in Fig. 7, the results are plotted in Figs. 8 and 9. Fig. 8 presents the nondimensional SIF versus the angle of positions of second crack, θ. Fig. 8 a shows that the values of F_1 for the crack tip A_1 when $R_2/R_1 =$ 0.1, 0.5, 0.9 have the maximum value at the angle $\theta = 82^\circ, 79^\circ$, and 79°, respectively. This result can be explained by observing that at each angle θ, the crack tip A_1 lies very closed to the second crack. In Fig. 8 b, there is a significant effect at $R_2/R_1 = 0.9$ as the angle θ increased. Fig. 8 c exhibits that the severity at the crack tip B_1 is significant at the angle $\theta = 79^\circ$ for the case $R_2/R_1 = 0.9$. From the data in Fig. 8 d, it is apparent that the nondimensional SIFs fluctuate as the angle θ increased. This result has shown that the second crack has a strong shielding effect on the crack tip B_2.

Fig. 9 shows the graphs of nondimensional SIF versus the ratio R_2/R_1. For $\theta = 180^\circ$, there has been a slight change of the nondimensional SIF values at the first (9 a and 9 b) and second cracks tips (9 c and 9 d) as the ratio R_2/R_1 increased.

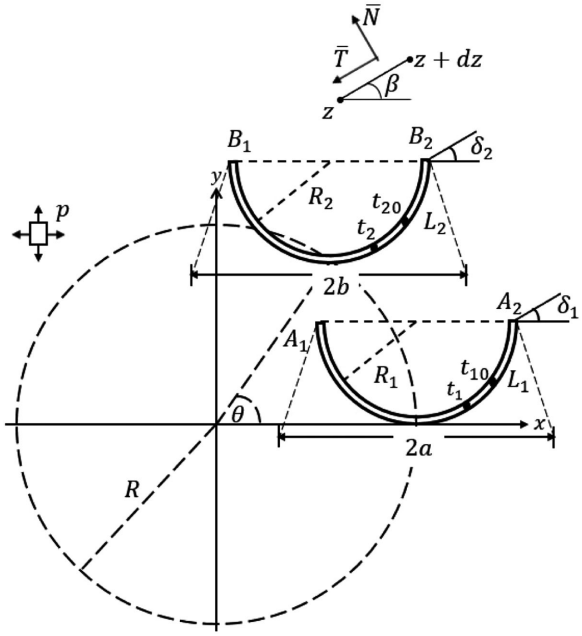

Fig. 7 Two curved cracks placed in a circular position in plane elasticity.

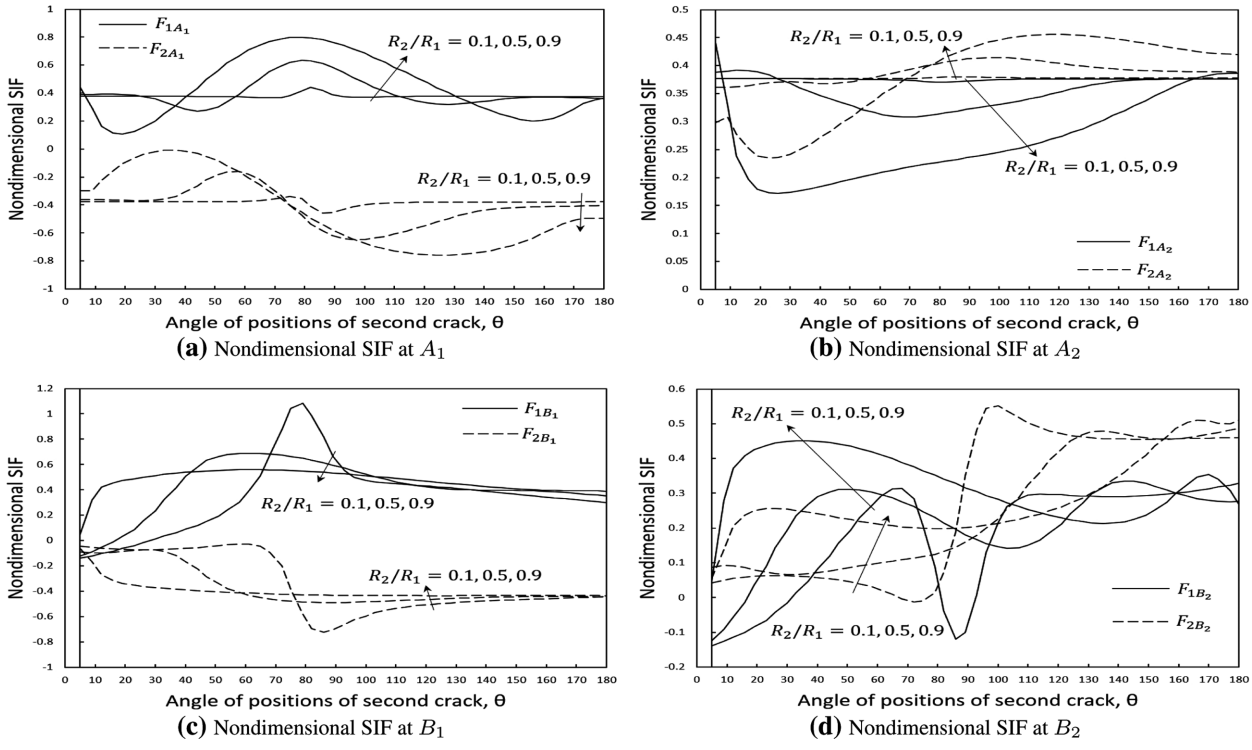

(a) Nondimensional SIF at A_1

(b) Nondimensional SIF at A_2

(c) Nondimensional SIF at B_1

(d) Nondimensional SIF at B_2

Fig. 8 Nondimensional SIF for two curved cracks as θ varies (Fig. 7).

This observation shows that at an angle $\theta = 180^\circ$, the severity at both curved cracks tips is not significant. In Figs. 9 a and 9 b, the effect at $\theta = 90^\circ$ on the value of F_1 is higher than $\theta = 55^\circ$. From Fig. 9 c, as $R_2/R_1 \geq 0.34$, the effect at $\theta = 55^\circ$ on the value of F_1 is higher than $\theta = 90^\circ$, and in Fig. 9 d, the effect at $\theta = 55^\circ$ on the value of F_1 is higher than $\theta = 90^\circ$ as R_2/R_1 increased.

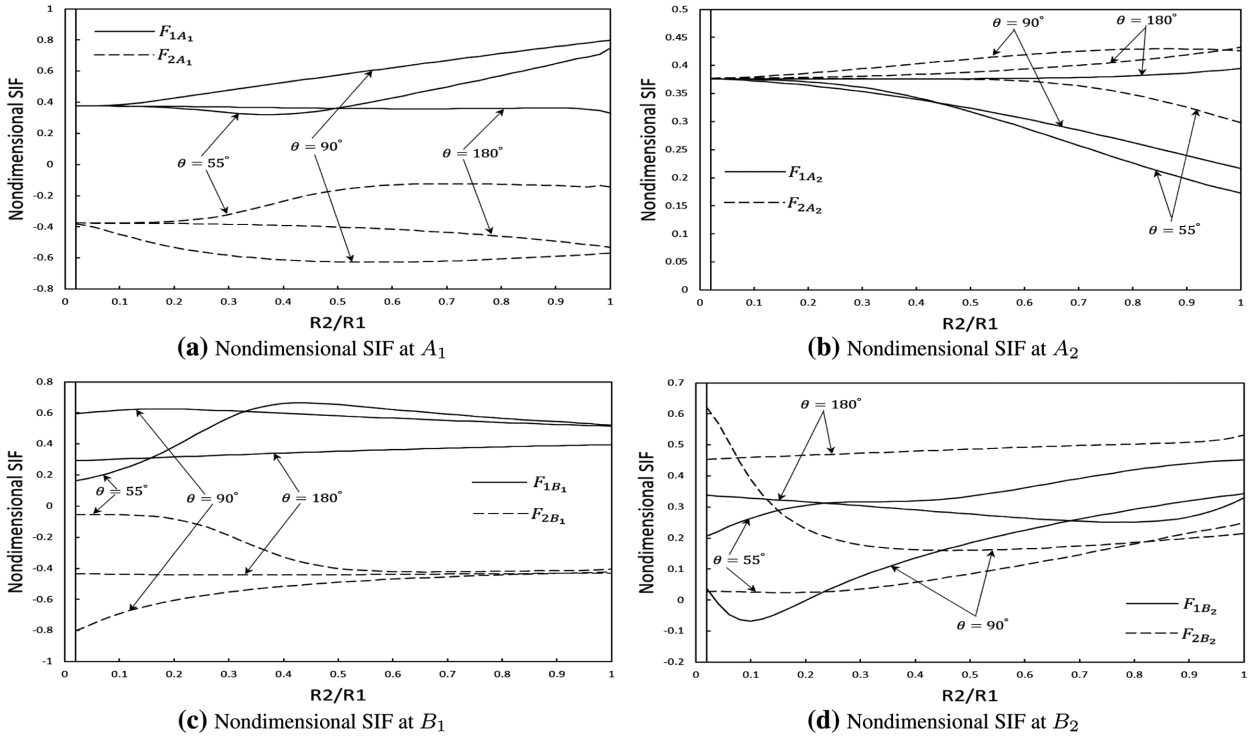

(a) Nondimensional SIF at A_1 **(b)** Nondimensional SIF at A_2

(c) Nondimensional SIF at B_1 **(d)** Nondimensional SIF at B_2

Fig. 9 Nondimensional SIF for two curved cracks when R_2/R_1 changing (Fig. 7).

3.3 Example 3

Consider the interaction between curve and inclined crack with length $2a$ and $2b$, respectively, in circular positions (Fig. 10). The remote tension is $\sigma_x^\infty = \sigma_y^\infty = p$. The calculated results for the SIFs at the crack tips A_1, A_2, B_1, and B_2 are

$$\begin{aligned} K_{iA_j} &= F_{iA_j}(\theta)p\sqrt{\pi a}, \\ K_{iB_j} &= F_{iB_j}(\theta)p\sqrt{\pi b}, \quad i, j = 1, 2. \end{aligned} \tag{17}$$

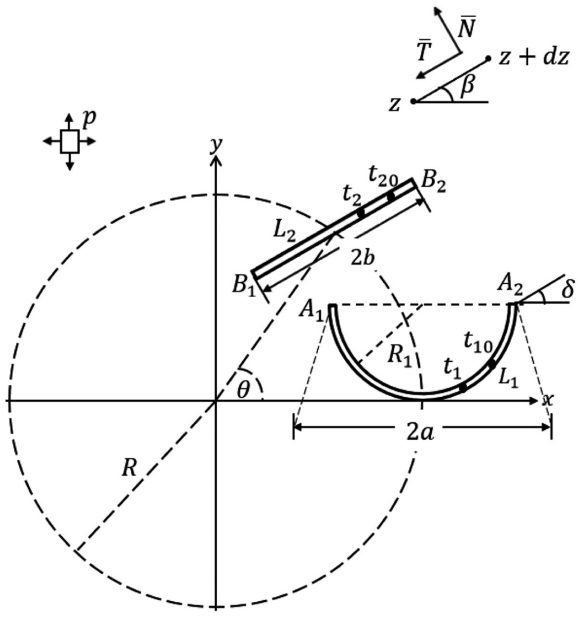

Fig. 10 Curved and inclined cracks placed in a circular position in plane elasticity.

Fig. 11 demonstrates the nondimensional SIF versus the angle of positions of second crack, θ, for $\alpha = 20^\circ$. Fig. 11 a presents the nondimensional SIFs for $b/R_1 = 0.1$ and $\delta = 85^\circ$ at the angle $6^\circ \le \theta \le 180^\circ$. The result shows that the shielding effect on the crack tips of inclined crack (B_1 and B_2) is most obvious at $40^\circ < \theta < 120^\circ$, but then less significant effect on the curved crack tips (A_1 and A_2) as θ increased. The highest value of F_{1B_1} is found at the angle $\theta = 90^\circ$ with the value $F_{1B_1} = 1.46010$, while for F_{1B_2} the same phenomenon happen at $\theta = 99^\circ$ with the value $F_{1B_2} = 1.42263$. Fig. 11 b exhibits the nondimensional SIFs for the ratio $b/R_1 = 0.5$ and $\delta = 45^\circ$ at the angle $30^\circ \le \theta \le 180^\circ$. As $\theta < 130^\circ$, the shielding effect on the inclined crack is significant. Meanwhile, the effect on the curved crack is more obvious on the crack tip A_1 than A_2 as θ increased. Figs. 11 c and 11 d show the nondimensional SIFs for the ratio of $b/R_1 = 0.9$ and 1.0, respectively, when $\delta = 45^\circ$ at the angle $36^\circ \le \theta \le 180^\circ$. Since the angle θ is varied, the shielding effect on the curved and inclined cracks is easily seen. However, the value of SIF at the right crack tip of inclined crack (B_1) is not significant as the angle θ increased.

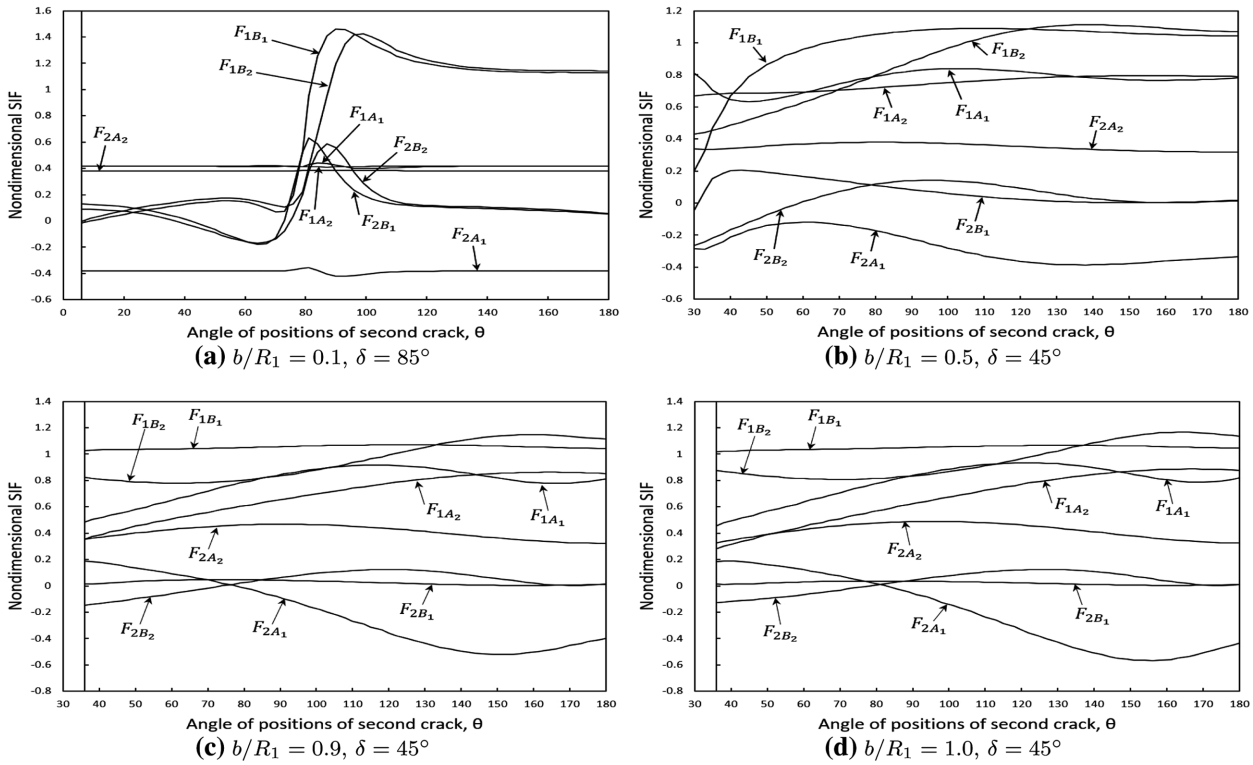

(a) $b/R_1 = 0.1$, $\delta = 85^\circ$ **(b)** $b/R_1 = 0.5$, $\delta = 45^\circ$

(c) $b/R_1 = 0.9$, $\delta = 45^\circ$ **(d)** $b/R_1 = 1.0$, $\delta = 45^\circ$

Fig. 11 Nondimensional SIF for $\alpha = 20^\circ$ when θ changing.

Fig. 12 illustrates the nondimensional SIF against the ratio b/R_1 for $\alpha = 30^\circ$ where the SIF at the crack tips are defined as

$$\begin{aligned} K_{iA_j} &= F_{iA_j}(a/R_1)p\sqrt{\pi a}, \\ K_{iB_j} &= F_{iB_j}(b/R_1)p\sqrt{\pi b}, \quad i, j = 1, 2. \end{aligned} \tag{18}$$

Figs. 12 a and 12 b have a similar pattern of nondimensional SIF. They show that the values of F_{1A_1} and F_{1A_2} are gradually decreased, while the values of F_{1B_1} and F_{1B_2} are gradually increased. These observations show that, as the ratio b/R_1 increased, the severity at the inclined crack tips is significant compared to the effect on the curved crack tips. In Fig. 12 c, it is found that the values of F_{1B_1} and F_{1B_2} take rather higher value than the values of F_{1A_1} and F_{1A_2}. In addition, the inclined crack tips are more severe at $b/R_1 = 0.02$. Fig. 12 d depicts the severity on the cracks tips at the angle $\theta = 180^\circ$ is not significant as the ratio b/R_1 increased.

4 Conclusion

The multiple cracks problems in a circular position in plane elasticity are studied. The hypersingular integral equation for two cracks have been formulated. The numerical examples showed the behaviour of the stress state at the crack tips. Since

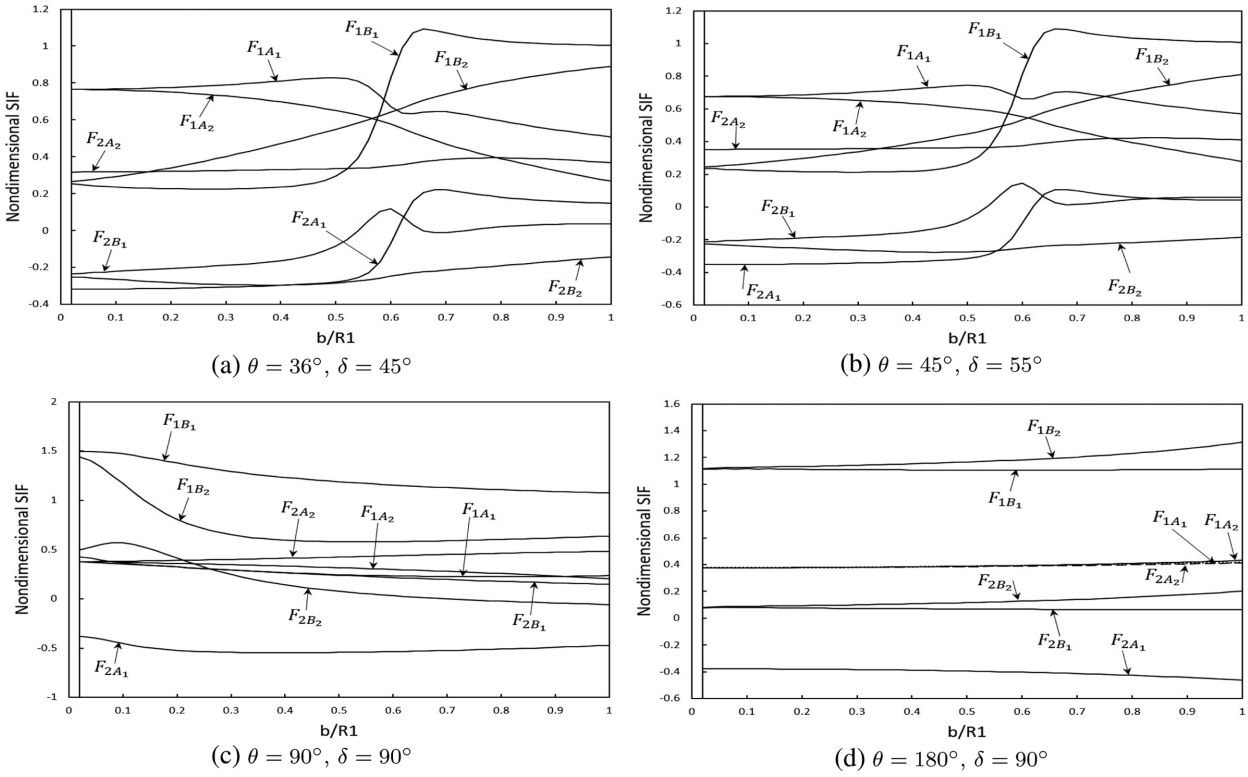

(a) $\theta = 36^\circ$, $\delta = 45^\circ$ (b) $\theta = 45^\circ$, $\delta = 55^\circ$

(c) $\theta = 90^\circ$, $\delta = 90^\circ$ (d) $\theta = 180^\circ$, $\delta = 90^\circ$

Fig. 12 Nondimensional SIF for $\alpha = 30^\circ$ when b/R_1 changing.

the angle θ is varied, it is obvious that the second crack tips is most affected than the first crack tips. In addition, with an increase of the length ratio of the second to the first crack, the shielding effect for the cracks at the angle $\theta \leq 90^\circ$ is obvious.

Acknowledgement The first author would like to thank Universiti Putra Malaysia (UPM), Malaysia for the Putra Grant, Vot No. 9442300.

Appendix

The following integration rules for the hypersingular and regular integrals, respectively, is very effective to solve the present problem [4].

$$\frac{1}{\pi} \oint_{-a}^{a} \frac{\sqrt{a^2 - s^2} G(s)}{(s - s_0)^2} ds = \sum_{j=1}^{M+1} W_j(s_0) G(s_j), \quad (|s_0| < a), \tag{A1}$$

$$\frac{1}{\pi} \int_{-a}^{a} \sqrt{a^2 - s^2} G(s) ds = \frac{1}{M+2} \sum_{j=1}^{M+1} (a^2 - s_j^2) G(s_j), \tag{A2}$$

where $G(s)$ is a given regular function, $M \in \mathbb{Z}$,

$$s_j = s_{0_j} = a \cos\left(\frac{j\pi}{M+2}\right), \quad j = 1, 2, 3, ..., M+1,$$

and

$$W_j(s_0) = -\frac{2}{M+2} \sum_{n=0}^{M} (n+1) V_j^n U_n\left(\frac{s_0}{a}\right),$$

where

$$V_j^n = \sin\left(\frac{j\pi}{M+2}\right)\sin\left(\frac{(n+1)j\pi}{M+2}\right).$$

Here $U_n(t)$ is a Chebyshev polynomial of the second kind, defined by

$$U_n(t) = \sin\left(\frac{(n+1)\theta}{\sin\theta}\right), \quad t = \cos\theta.$$

$H_1(s)$ and $H_2(s)$ can be evaluated using

$$H_1(s) = \sum_{n=0}^{M} c_{1n} U_n\left(\frac{s}{a}\right), \quad |s| \le a, \tag{A3}$$

and

$$H_2(s) = \sum_{n=0}^{M} c_{2n} U_n\left(\frac{s}{b}\right), \quad |s| \le b, \tag{A4}$$

where

$$c_{1n} = \frac{2}{M+2}\sum_{j=1}^{M+1} V_j^n H_1(s_1), \quad c_{2n} = \frac{2}{M+2}\sum_{j=1}^{M+1} V_j^n H_2(s_2), \tag{A5}$$

and $H_1(s_1)$ and $H_2(s_2)$ are defined from Eqs. (10) and (11), respectively.

References

[1] N. I. Muskhelishvili, Some Basic Problems of the Mathematical Theory of Elasticity (Noordhoff International Publishing, Leyden, 1953).
[2] Y. Z. Chen, N. Hasebe, and K. Y. Lee, Multiple Crack Problems in Elasticity (WIT Press, Southampton, 2003).
[3] N. M. A. Nik Long and Z. K. Eshkuvatov, Hypersingular integral equation for multiple curved cracks problem in plane elasticity, Int. J. Solids Struct. **46**, 2611–2617 (2009).
[4] K. Mayrhofer and D. Fisher, Derivation of a new analytical solution for a general two dimensional finite-part integral applicable in fracture mechanics, Int. J. Numer. Meth. Eng. **33**, 1027–1047 (1992).
[5] N. M. A. N. Long, M. R. Aridi, and Z. K. Eshkuvatov, Mode stresses for the interaction between an inclined crack and a curved crack in plane elasticity, Math. Probl. Eng. (2015).
[6] F. Erdogan, On the stress distribution in plates with collinear cuts under arbitrary loads, Proc. 4th U.S. Nat. Congr. Appl. Mech., 547–553 (1962).
[7] M. Denda and Y. F. Dong, Complex variable approach to the BEM for multiple crack problems, Comput. Methods Appl. Mech. Eng. **141**, 247–264 (1997).
[8] G. Vialaton, G. Lhermet, G. Vessiere, M. Boivin, and J. Bahuaud, Field of stresses in an infinite plate containing two collinear cuts loaded at an arbitrary location, Eng. Fract. Mech. **8**, 525–538 (1976).
[9] V. V. Panasyuk, M. P. Savruk, and A. P. Datsyshyn, A general method of solution of two-dimensional problems in the theory of cracks, Eng. Fract. Mech. **9**, 481–497 (1977).
[10] M. Kachanov, A simple technique of stress analysis in elastic solids with many cracks, Int. J. Fract. **28**, R11–R19 (1985).
[11] M. Kachanov, Elastic solids with many cracks: A simple method of analysis, Int. J. Solids Struct. **23**(1), 23–43 (1987).
[12] Y. Z. Chen, Singular integral equation method for the solution of multiple curved crack problems, Int. J. Solids Struct. **41**, 3505–3519 (2004).
[13] Y. Z. Chen and X. Y. Lin, Numerical solution of singular integral equation for multiple curved branch-cracks, Struct. Eng. Mech. **34**, 85–95 (2010).
[14] J. Helsing, A fast and stable solver for singular integral equations on piecewise smooth curved, SIAM J. Sci. Comput. **33**, 153–174 (2011).
[15] Y. Z. Chen, General case of multiple crack problems in an infinite plate, Eng. Fract. Mech. **20**, 591–597 (1984).
[16] Y. Z. Chen, New Fredholm integral equation for multiple crack problem in plane elasticity and antiplane elasticity, Int. J. Fract. **64**, 63–77 (1993).
[17] Y. Z. Chen, A survey of new integral equations in plane elasticity crack problem, Eng. Fract. Mech. **51**, 97–134 (1995).
[18] Y. Z. Chen, Hypersingular integral equation approach for the multiple crack problem in an infinite plate, Acta Mech. **108**, 121–131 (1995).
[19] Y. Z. Chen, A numerical solution technique of hypersingular integral equation for curved cracks, Commun. Numer. Meth. Eng. **19**, 645–655 (2003).
[20] M. R. Aridi, N. M. A. N. Long, and Z. K. Eshkuvatov, Mode stresses for the interaction between straight and curved cracks problem in plane elasticity, J. Appl. Math. Phys. **2**, 225–234 (2014).

[21] V. V. Zozulya, Regularization of hypersingular integrals in 3-D fracture mechanics: Triangular BE, and piecewise-constant and piecewise-linear approximations, Eng. Anal. Bound. Elem. **34**, 105–113 (2010).
[22] X. Wang, W. T. Ang, and H. Fan, Hypersingular integral and integro-differential micromechanical models for an imperfect interface between a thin orthotropic layer and an orthotropic half-space under inplane elastostatic deformations, Eng. Anal. Bound. Elem. **52**, 32–43 (2015).
[23] Y. Z. Chen, Numerical solution of a curved crack problem by using hypersingular integral equation approach, Eng. Fract. Mech. **46**(2), 275–283 (1993).
[24] Y. Z. Chen, Hypersingular integral equation for multiple crack problem in an infinite plate, Acta Mech. **108**, 121–131 (1995).
[25] Y. Z. Chen and N. Hasebe, Hypersingular integral equation for a curved crack problem of circular region in antiplane elasticity, ASME J. Appl. Mech. **63**, 845–849 (1996).
[26] Y. Z. Chen, Numerical solution of circular cracked plate problem by using hypersingular integral equation approach, Com. Numer. Meth. Eng. **14**, 451–461 (1998).
[27] Y. Z. Chen, X. Y. Lin, and Z. X. Wang, Numerical solutions of hypersingular integral equation for antiplane elasticity curved crack problems of circular regions, Acta Mech. **173**, 1–11 (2004).
[28] Y. Z. Chen, Numerical solutions of hypersingular integral equation for curved cracks in circular regions, Inter. J. Fract. **132**(3), 205–222 (2005).
[29] Y. Z. Chen, X. Y. Lin, Z. X. Wang, and N. M. A. N. Long, Solution of contact problem for an arc crack using hypersingular integral equation, Int J. Comut. Methods **5**(1), 119–133 (2008).
[30] Y. Z. Chen, X. Y. Lin, and Z. X. Wang, Numerical solution for curved crack problem in elastic half-plane using hypersingular integral equation, Philos. Mag. **86**(26), 2239–2253 (2009).

